

# **Deep convective cloud top heights and their thermodynamic control during CRYSTAL-FACE**

Steven C. Sherwood

Department of Geology and Geophysics, Yale University, New Haven, CT, USA

Patrick Minnis

NASA/Langley Research Center, Hampton, Virginia

Matthew McGill

NASA/Goddard Space Flight Center, Greenbelt, Maryland

Short title: CLOUD TOP HEIGHTS

**Abstract.** Infrared ( $11\ \mu\text{m}$ ) radiances from GOES-8 and local radiosonde profiles, collected during the Cirrus Regional Study of Tropical Anvils and Cirrus Layers- Florida Area Cirrus Experiment (CRYSTAL-FACE) in July 2002, are used to assess the vertical distribution of Florida-area deep convective cloud top height and test predictions as to its variation based on parcel theory. The highest infrared tops ( $Z_{11}$ ) reached approximately to the cold point, though there is at least a 1-km uncertainty due to unknown cloud-environment temperature differences. Since lidar shows that visible “tops” are 1 km or more above  $Z_{11}$ , visible cloud tops frequently penetrated the lapse-rate tropopause ( $\sim 15$  km). Further, since lofted ice content may be present up to  $\sim 1$  km above the visible tops, lofting of moisture through the mean cold point (15.4 km) was probably common. Morning clouds, and those near Key West, rarely penetrated the tropopause. Non-entraining parcel theory (i.e., CAPE) does not successfully explain either of these results, but can explain some of the day-to-day variations in cloud top height over the peninsula. Further, moisture variations above the boundary layer account for most of the day-to-day variability not explained by CAPE, especially over the oceans. In all locations, a 20% increase in mean mixing ratio between 750 and 500 hPa was associated with about 1 km deeper maximum cloud penetration relative to the neutral level. These results suggest that parcel theory may be useful for predicting changes in cumulus cloud height over time, but that parcel entrainment must be taken into account even for the tallest clouds. Accordingly, relative humidity above the boundary layer may exert some control on the height of the tropical troposphere.

## 1. Introduction

In the Tropics, sufficient conditional instability is usually present for clouds to reach through most of the upper troposphere, at least according to non-entraining parcel theory. In fact, over the tropical western Pacific, it is true almost 90% of the time that CAPE (convective available potential energy) exceeds that of the “neutral” state toward which convection drives the column [Sherwood, 1999]. Tropical clouds are frequently observed to reach within a few kilometers of the tropopause, particularly in high-CAPE environments [e.g. Jensen and Del Genio, 2003]. It is generally assumed that greater quantities of CAPE—the kinetic energy that a non-entraining, near-surface parcel can attain through lofting—will lead to stronger convection. Measures of strength include greater updraft velocities and greater cloud-top heights. Estimated cloud heights serve as a proxy for convective strength and precipitation with reasonable success, as predicted by simple models [e.g. Adler and Negri, 1988].

It is clear from previous measurements, however, that typical updraft velocities fall far short of the theoretical maxima, especially over oceans where the shortfall is typically more than an order of magnitude [Jorgensen and Lemone, 1989; Lucas *et al.*, 1994]. This indicates that energy conversion is often inefficient. The inefficiency is probably due to entrainment dilution and/or retention of condensed liquid in updrafts [e.g. Jorgensen and Lemone, 1989], although non-hydrostatic pressure effects could also play a role [Chen and Sun, 2002]. Simple cloud models that include these effects have been judged successful in predicting cloud top heights and water content in case studies [Ferrier and Houze, 1989].

An understanding of what controls convective intensity is of interest for a number of reasons. For example, intense updrafts are responsible for the creation of hailstones and lightning. Lightning appears to require updraft strengths which, although well below those predicted for a pseudo-adiabatic parcel, are greater than those actually achieved over oceans most of the time [Zipser and Lutz, 1994]. Thus, the efficiency with which CAPE is realized is a key factor in regulating lightning and other severe storm characteristics. Further, considerable interest has developed in quantifying the extent of cloud penetration near the tropopause, to estimate in turn the degree of convective mixing or other effects at levels close to or within the

lower stratosphere [e.g. *Alcala and Dessler, 2002; Gettelman et al., 2002*]. Such mixing may cause transport of pollutants into the stratosphere [*Fromm and Servranckx, 2003*] and influence tropopause temperatures [*Sherwood et al., 2003*] and moisture. Understanding is hampered by poor understanding of both convective intensity and cloud-top dynamics. *Sherwood and Dessler* [2001], for example, found that overshooting cloud tops could dominate the water budget in the last stages of stratospheric entry, but their model optimistically assumed that a nontrivial percentage of convective drafts would come close to attaining full thermodynamic efficiency. This may be unrealistic, but on the other hand, it is possible that some cloud water may be lofted well above the apparent cloud top, in amounts small by tropospheric standards but significant for the stratosphere.

Although typical updraft speeds are far below those predicted for an idealized parcel, the distribution of updraft speed is known to have a long tail, such that a few drafts are much stronger than average [*Yuter and Houze, 1995*]. Since they are so rare, it is not clear from current data how well the behavior of the strongest updrafts may be controlled by parcel buoyancy in the prestorm environment. Though small in terms of storm area, the most intense drafts will likely dominate whatever role convection may play in mixing near the base of the stratosphere (a region that is otherwise very quiescent, with long dynamical and radiative time scales). Likewise, we may expect the tail of the cloud-height distribution to be more important than “average” heights. Study of this tail requires extensive sampling, for example by geostationary imagery.

In July 2002, the CRYSTAL-FACE (Cirrus Regional Study of Tropical Anvils and Cirrus Layers-Florida Area Cirrus Experiment) employed numerous aircraft, surface, and space-based platforms to investigate the growth and decay of upper-tropospheric cloud decks [*Jensen et al., 2003*]. Here, we characterize the distribution of deep convective cloud-top heights that occurred during this experiment. We make no attempt to explain variations in the amount of convective activity, nor analyze individual cases using radar vertical velocity data (whose availability is more limited than radiometric cloud-top data). Case studies of individual CRYSTAL convective events have been undertaken by *Li* [2003].

## 2. What is the “cloud top”?

This question is not as simple as it seems. Our common experience is with clouds whose boundaries are either visibly sharp (liquid water cumulus clouds) or not easily visible at all (stratiform clouds). Though we might expect glaciated, deep convective clouds to have optically sharp tops too, this is not born out by lidar observations.

Figure 1 shows data from the NASA Goddard Cloud Physics Lidar (CPL) on board the ER-2 high altitude research aircraft. Each lidar dwell that encountered a deep convective cloud was composited relative to the level  $Z_{\text{lid}}(1)$  at which the optical depth (found by integrating the visible extinction) was equal to unity; such composites were developed for several brightness temperature ranges corresponding to different cloud heights in the upper troposphere. The  $Z_{\text{lid}}(1)$  level is the most sensible definition of a radiometric “cloud top,” since it lies at the mean penetration depth of a (visible) photon.

The figure shows two interesting things. First, cloud water content decays exponentially above  $Z_{\text{lid}}(1)$  with an  $e$ -folding distance of about 200 meters. This decay continues for quite a few cloud “scale heights” with no significant change in slope, a fact of potential importance for stratospheric water vapor. A typical mixing ratio of the latter is 5 ppmv which corresponds, at 100 hPa altitude, to a volumetric extinction coefficient of about  $5 \times 10^{-5} \text{m}^{-1}$  assuming cloud particle diameters near 20-30 microns. This extinction level, indicated in Figure 1, lies on average at least one kilometer above  $Z_{\text{lid}}(1)$ . Since clouds condensed in situ by lofting above the cloud top (pileus clouds) must have ice water concentrations well below the ambient water vapor concentration, the extinctions observed up to 1 km above  $Z_{\text{lid}}(1)$  must result primarily from condensation within tropospheric air lofted by the storm.

The second interesting feature, indicated schematically in Figure 1 based on the results of *Heymsfield et al.* [1991] and *Sherwood et al.* [2004], is that the GOES radiometric cloud top  $Z_{11}$  colocated with the lidar retrievals lies at least 1 km below  $Z_{\text{lid}}(1)$ . Those authors were unable to explain this discrepancy, but both studies noted that it was common to more than one infrared imager, so it is unlikely to be an instrument problem.

Taken together, these facts indicate that true “cloud top” (defined in terms of visible

opacity) must lie at least 1 km above—and stratospherically significant water vapor must typically be lofted to perhaps 2 km above—the cloud tops seen by GOES-8. Since these errors and/or processes are not well understood, we do not attempt to model them in any way beyond treating them as constant biases or offsets. This must be constantly kept in mind when interpreting the GOES  $Z_{11}$  data. Further work will be necessary to learn what factors control the size of these height differences.

### 3. Computation of thermal Cb heights

To obtain reasonable statistics we must rely upon GOES-8 for cloud top height information, subject to the caveats noted above. To obtain  $Z_{11}$ , the cloud “top” height according to passive radiances near 11 microns, we match brightness temperatures  $T_{11}$  obtained from GOES radiances to inferred temperature profiles (see below). The  $T_{11}$  were obtained from 4-km infrared ( $10.8 \mu\text{m}$ ) observations every 15 minutes by the eighth Geostationary Operational Environmental Satellite (GOES-8). Calibration of the GOES-8 infrared radiances is maintained using on-board blackbodies. The GOES-8 data have also been compared with radiances from similar channels on two research satellites [Minnis *et al.*, 2002] and agree to within  $\pm 0.5$  K over the full range of temperatures, on average. Cloud heights were determined by methods described by Sherwood *et al.* [2004], repeated here.

#### 3.1. Regions and satellite-sounding matching

We computed  $Z_{11}$  statistics over three regions: the PEN or Florida peninsula region (roughly the mainland south of Tampa), the KW or Key West region (the Keys plus nearby ocean), and the FAGA or Florida-area Gulf/Atlantic Ocean region not included in KW. Each region is shown in Figure 2. A reference temperature profile was computed for each region and time as follows. For the KW region, the Key West sounding taken at the nearest available observing time was used; for the PEN region, the soundings from Miami, the Western Ground site, and Tampa at the nearest available observing time were averaged; and for the FAGA region, all four stations were averaged. The temperature profile for FAGA is therefore not

expected to faithfully represent details of local atmospheric stability and CAPE. However, since contemporaneous temperatures above the boundary layer did not differ much among the stations, significant cloud height errors are unlikely from temperature variability, and should be almost as good in FAGA as the other regions. The mean temperature sounding from the experiment is shown in Figure 3.

The “nearest available observing time” is taken to be the closest time of day at which there is at least one observation available from the station(s) in question. If no observations were available the entire day (which was the case for the first and last days of the month), then an average was taken of soundings within two days of the target time. Finally, for purposes of finding  $Z_{11}$  the temperature profiles were smoothed slightly in the vertical using a moving weighted window of width 15 hPa, to reduce features comparable to or smaller than a photon mean free path.

### 3.2. Cloud temperature assumption

A height  $Z_{11}$  was computed for each GOES-8 pixel using the appropriate reference profile. Typically, one simply assigns the pressure and altitude where the profile matches the 11 micron brightness temperature  $T_{11}$  (the level nearest the surface is used if there is more than one match). This implies an assumption that the cloud temperature will be the same as that of a distant environment at the same altitude. Through most of the troposphere, this is reasonable: while the interior of thermals tends to be several K warmer than the environment, this anomaly decreases toward cloud top due to adiabatic cooling and mixing. For overshooting convective clouds, however, adiabatic cooling is the dominant effect, and the cloud temperature should become colder than the environment, by as much as 20 K or more in extreme cases [e.g. *Adler and Mack*, 1986]. Indeed, some cloud-top temperatures in our dataset were colder than any point in the sounding, which demands an alternative  $T(Z)$  relation for the cloud.

Not knowing exactly how to do this, we tried three candidate procedures. The first, or “adiabatic-1” profile involved replacing temperatures above the WMO (lapse-rate) tropopause with an adiabat intersecting the observed profile at the tropopause level. The “adiabatic-2”

profile was identical except starting 40 hPa below the WMO tropopause, found to be a sufficient distance so that the the lapse rate is fairly close to an adiabat and cloud buoyancies are more likely to be neutral. Finally we consider a “semiadiabatic” profile which is just the average the adiabatic-2 and environmental temperature profiles, representing the likely result of a cloud actively mixing with its environment. The differences among these serve as an uncertainty measure, although they do not necessarily bracket all possibilities.

#### 4. Observed cloud height and sounding variations

Cloud top heights might be expected to reflect the ability of near-surface air parcels to ascend. A near-surface parcel in the summertime Florida environment typically can achieve positive buoyancy if lifted a small distance above its starting level; when the buoyancy returns to zero again, the parcel has ascended to its level of neutral buoyancy or LNB. On its way to this level, the potential energy available for conversion to kinetic energy is the CAPE. If all this energy is converted back to potential energy again during an overshoot, then the parcel eventually comes to rest at the level of maximum overshoot or LMO, the highest attainable level in parcel theory. In practice, most of the CAPE for most parcels is consumed on the way up through mixing with the environment, but some parcels may occasionally achieve high conversion efficiencies. Here, these quantities are calculated assuming a pseudo-adiabatic, irreversible ascent. Latent heat of fusion to the ice phase is neglected, but has been shown to approximately compensate for the gravitational loading of condensate [*Williams and Renno, 1993*] which is also neglected.

We now report uncorrected height variations observed by GOES, together with CAPE, LNB, etc. For the most part these will be reported as pressure ( $p_{11}$ ) values, since the soundings measure pressure, but equivalent heights  $Z_{11}$  will be used interchangeably in the discussion (the  $p(Z)$  relation varied little over the experiment). Readers should keep in mind that visible cloud-top heights are probably at least 1 km higher than  $Z_{11}$  (perhaps 2 km for the tallest examples), while significant amounts of condensed water may exist up to another kilometer above that. While a correction could have been incorporated into our plots by simply adding

1 km to each estimated height, we are loath to do this without understanding the error better. Future work with MISR, IR, and laser altimeter data will undoubtedly reveal more about the nature of these errors.

#### 4.1. Height distributions

The distribution (histogram) of GOES  $p_{11}$  is shown in Fig. 4 within each of the three regions. Also shown are vertical distributions of LNB and LMO, and the WMO tropopause and cold point mean locations, for each region. LNB and LMO were calculated for each air parcel between the surface and 900 hPa (at 20 hPa resolution) in order to compute this distribution; parcels nearest the surface are most likely to have the greatest values. CAPE was calculated pseudo-adiabatically using an undilute parcel; calculations with other assumptions about condensate retention cause the distributions to move slightly upward or downward.

Clouds penetrated deepest over the peninsula (PEN). The histograms quickly begin falling off near 14 km (about 1 km below the WMO tropopause), but  $Z_{11}$  reached above the mean cold point height (15.5 km) in the most extreme cases. Different  $T(Z)$  models lead to about a 1 km range in the extreme heights, causing the cold-point penetration frequency (based on  $Z_{11}$ ) to range from about 0.01% to 1% of that at 14 km (which is not sensitive to the  $T(Z)$  model). In view of the biases noted above, however, we presume that the falloff in visible cloud top heights began right around the lapse-rate tropopause or cold point. This implies much more frequent cloud penetration of these levels than the values quoted above. Further, we may infer that stratospherically significant ice concentrations were occasionally inserted to heights up to 2 km above the cold point, or  $\sim 17$  km. It is obviously difficult to be quantitative about cloud penetrations of the tropopause in the face of such large uncertainties in  $Z_{11}$  and its interpretation.

The LNB distribution in PEN matches that of  $Z_{11}$  fairly well, which implies that visible tops typically reached 1-2 km above the LNB. The LMO distribution peaked broadly near 100 hPa and reached as high as 19 km, greater than any observed height even taking biases into account, which probably indicates that no overshoots penetrated all the way to the theoretical

LMO of a non-entraining parcel. However, given the apparent tendency of GOES to saturate toward the tallest clouds, it is hard to rule out very deep cloud penetrations with certainty.

In the Key West (KW) region, the  $Z_{11}$  histogram resembles that over the peninsula except for a downward shift of about 1 km. Cloud-top frequencies begin falling off near 13 rather than 14 km, exhibiting a slightly more gradual or “rounded” falloff at first but achieving peak heights at least one kilometer lower than those over the peninsula. This difference persisted despite the fact that the average CAPE, LNB, and tropopause height were about the same. In fact, the tropopause and cold point were each slightly higher over KW. The reasons for the lesser cloud heights are not clear, but the difference is consistent with previous findings [Jorgensen and Lemone, 1989; Lucas *et al.*, 1994] that updraft speeds are greater in general for continental than for oceanic convection. It is particularly interesting that both regions possess histogram “bends,” but at altitudes that do not seem simply related to the tropopause or LNB.

Cloud heights over the other nearby oceans (FAGA) were in between those of Key West and the peninsula. It is not clear why Key West cloud heights were depressed relative to other oceanic areas, though one likely possibility is that Key West is relatively close to the peninsula, whose stronger convection may inhibit that over nearby oceans. Due to the lack of sounding data over the oceans, it is not possible to assess differences in stability between these regions and Key West.

## 4.2. Diurnal cycle

Diurnal cycles of several quantities are shown for each region in Fig. 5. To produce a mean CAPE value for a particular time of day, we averaged all parcel values that were greater than 100 J/kg (reckoning that other parcels would not participate in convection; results are similar, but with a lower mean, if all parcels are included). The diurnal variations of CAPE are small, with a slight peak in the late morning, while cloud height shows a strong afternoon peak over PEN. Thus, the huge diurnal variation in cloud height over land is not explained at all by CAPE. The CAPE variations themselves are readily explained by solar heating and convective effects, with an afternoon dip accompanying the downward transport of cool air by convection.

The true explanation of the diurnal cycle in convective coverage and penetration evidently involves mesoscale dynamics. Sea-breeze fronts are created at the Florida coastlines, and propagate inward as density currents, eventually colliding and producing strong convection through a localized lifting effect [Burpee, 1979; Burpee and Lahiff, 1984]. This enhancement may also produce the higher clouds relative to the KW region. There are, however, several other factors that may contribute more generally to a broad and well-observed (but as yet not fully explained) difference between land and ocean convective intensity under similar CAPE situations [see Lucas *et al.*, 1994]. It is likely that modeling studies will be necessary to unravel the causes of this in general.

### 4.3. Day-to-day variations

CAPE variations appear to be somewhat more successful in accounting for daily-mean variations through the month within a given region (Figure 6). Daily means of parcel properties are again calculated by averaging over all buoyant, low-level parcels. In addition to quantities examined earlier, we now include mean water vapor mixing ratios in the lower (750-500 hPa) and upper (500-250 hPa) free troposphere. These mixing ratios include corrections for lag and bias errors [Miloshevich *et al.*, 2004].

Several patterns of behavior previously noted for tropical convection are evident. First, greater amounts of convection (top row) appear to coincide with (i) higher upper-tropospheric water vapor (top row), probably due to increased supply of water vapor to these levels by convection; (ii) deeper penetration (middle row), presumably due to a natural correlation between system vigor and horizontal extent; and (iii) falling CAPE (bottom row), probably by limiting solar heating and transporting cool air toward the surface. These conclusions are insensitive to how CAPE is averaged or calculated. We have listed these associations in decreasing order of strength:  $dCAPE/dt$  and convective penetration height are only loosely correlated with convective coverage.

Most relevant to this study are those factors associated with convective penetration. CAPE appears to increase penetration somewhat as expected, though there are a number of

counterexamples (July 4 with high CAPE and modest  $Z_{11}$ , for example, or the 14th where the reverse occurred). Interestingly, while CAPE appears to minimize a day too early to explain the low  $Z_{11}$  on July 23, the 750-500 hPa moisture dips on just the same day as  $Z_{11}$ . Throughout the month, and in all regions, this moisture variable appears to track  $Z_{11}$  as well as, or better than, CAPE. While upper-tropospheric moisture mirrors deep convective coverage (top row of the figure, and is for example high on the 23rd), the 750-500 hPa moisture behaves differently and resembles cloud height more closely than cloud amount. This suggests that moisture variations are regulating cloud penetration in a way that is independent of variations in convective coverage or frequency.

The connection between CAPE and contemporaneous cloud heights is investigated more carefully in Figure 7, which compares peak  $p_{11}$  against two indices based on parcel theory. The first index is the LNB pressure, while the second is the mean of the LMO and LNB. The second quantity was inspired by the more detailed convective model employed by *Sherwood and Dessler* [2001], in which overshooting convective air masses are created in the levels between the LNB and LMO by a mixing process with the environment; in this theory, changes in the LMO and LNB should both contribute to changes in peak cloud heights.

The results confirm that the calculated LNB does (albeit loosely) track variations in observed cloud-top height, with about a one-to-one slope. The correspondence is best over PEN ( $r = 0.29$ ). Interestingly, it is about as good over FAGA if a single outlier is excluded, even though the LNB is based on coastal data; this is probably due to horizontal coherence in the meteorology that causes CAPE variations. However, correspondence is poor over Key West and virtually disappears if a single outlier is discarded from that dataset. This result makes sense if we accept the earlier explanation for why cloud tops were shallower over Key West—suppression from peninsular convection—since higher LNB's over Key West would correlate with higher ones over the peninsula and greater competition from convection there, potentially canceling out the local boost.

If the LMO is included in predicting the cloud height, the mean value is estimated correctly over PEN and the correlation improves too (to  $r = 0.38$ ). However, both the mean

and correlation deteriorate over the oceanic regions. This is consistent with the apparently weaker convection over oceans, since significant convective overshooting is necessary before the theoretical LMO can have any impact. The PEN correlations are significant at 95% confidence if each day is regarded as an independent event, but not when serial correlation is taken into account. Thus we have only limited evidence in support of parcel theory, even over the peninsula.

The relationship between mid-tropospheric moisture and  $Z_{11}$  is explored in Figure 8, where the difference between the parcel theory result (mean of LNB and LMO pressures) and  $p_{11}$  is plotted against moisture. These correlations are highly significant everywhere ( $r = -0.64$  for PEN, and almost as high for the oceanic regions, all significant at 95% confidence). This indicates that moisture above the boundary layer (which is not employed in the non-entraining CAPE formulation) accounts for most of the variations in  $Z_{11}$  that are not explained by LNB/LMO. The success even over FAGA, where the sounding data are much less representative, indicates that moisture above the boundary layer varies coherently enough over synoptic scales for the Florida soundings to capture much of the variation. While the LNB/LMO is the more skillful univariate predictor over the peninsula, moisture is far more skillful over the oceans. Together,  $(\text{LNB}+\text{LMO})/2$  and 750-500 hPa moisture explain about 30% of the day-to-day variance in  $p_{11}$  over the peninsula, and the moisture by itself explains 38% (with no significant additional skill from LNB/LMO) over Key West. These are impressive figures given the noise and small-scale structure affecting the sounding observations.

The role of mid-level moisture in regulating convective outbreak and development has been explored in a variety of recent studies [e.g. *Grabowski*, 2003; *Sherwood*, 1999; *Tompkins*, 2001]. This role is likely to be associated with the entrainment process, whose impact on parcel buoyancies depends on the relative humidity of the entrained air. Our results here are the first that we know of to report an apparent control of observed peak cloud-top heights by moisture above the boundary layer.

## 5. Conclusion

We have examined histograms of convective cloud height near the tropopause, with the general goal of examining the tail of this distribution and assessing its sensitivity to environmental stability. All results must be viewed in light of the fact that “cloud top” is a fuzzy concept for deep convective clouds. Visible cloud tops based on direct lidar observations [Heymsfield *et al.*, 1991; Sherwood *et al.*, 2004] lie about one km higher than infrared ones (designated  $Z_{11}$ ), perhaps up to 2 km higher for the tallest clouds. Further, cloud ice water significant for stratospheric moistening may be found up to another kilometer above the visible top. All conclusions here are based on converting  $Z_{11}$  to putative visible tops by adding a constant offset of 1 km.

Convective clouds penetrated about a kilometer deeper over the Florida peninsula than near Key West, with clouds elsewhere in the surrounding oceans falling in-between. Peninsular clouds also exhibited a very strong diurnal cycle, as is well known. Neither the diurnal nor geographic variations in penetration seem to have anything to do with atmospheric CAPE, instead reflecting variations in the efficiency with which CAPE is converted into updraft kinetic energy (or, possibly, variations in the contributions of latent heat of fusion or condensate loading to parcel buoyancy). Previous studies have argued that land convection is stronger due to sea-breeze interactions [e.g., Burpee and Lahiff, 1984], a deeper planetary boundary layer [Jorgensen and Lemone, 1989], aerosol influences on cloud microphysics [e.g., Williams *et al.*, 2002], and/or land surface elevation maxima [Souza *et al.*, 2000]. This question has not been fully resolved, though a consensus may be hoped for once regional numerical simulations incorporate sufficient microphysics, and become able to represent with sufficient fidelity the patterns to be explained.

On average, visible cloud tops over the peninsula were apparently located in between the LNB and LMO, and day-to-day fluctuations tracked those of both the LNB and LMO, although with considerable scatter. The discrepancies were well explained by humidity variations just above the boundary layer (750-500 hPa). Thus, we found no evidence of significant day-to-day changes in the CAPE utilization efficiency other than those associated

with moisture entrainment. Having said this, moisture effects appear to be significant: we find that a 20% decrease in humidity above the boundary layer reduces peak cloud heights by about one kilometer, for a given (non-entraining parcel) LNB. This is true also over oceans, where LNB variations are less relevant and LMO completely irrelevant. The overall prediction skill of the thermodynamic variables is encouraging, because it suggests that useful predictions of seasonal, interannual, and longer-term changes in cloud top heights may be possible based on parcel theory. It is likely, however, that entrainment effects would have to be taken into account. In particular, relative humidities in the lower free troposphere would appear to be able to regulate the mean height of convective outflow (important for upper tropospheric water vapor and its radiative feedback on climate change [e.g. *Hartmann and Larson, 2002*]) independently of changes in atmospheric stability.

Height variations between Key West and the peninsula remain an enigma. There are no significant differences in LNB, 750-500 hPa moisture, or tropopause height to explain them. It is interesting that the histograms of cloud height in the two regions are so similarly shaped except for the 1-km offset. For example, both show a quick bend toward lower frequencies above a certain altitude. One might expect the bend to be associated with increasing static stability near the tropopause—but this cannot be the case, as the bend altitude varied significantly with location, while the tropopause varied much less and in the opposite direction. Instead, the rough coincidence between the heights of steep lapse-rate change and convective tops is probably because of convective control of temperatures rather than stability-imposed convective “ceilings” [cf. *Kuang and Bretherton, 2004; Sherwood and Dessler, 2001; Sherwood et al., 2003*]. Although stability clearly must affect convective growth, parcel buoyancy is determined by the vertical integral of stability rather than by its local value, so it should not be surprising that we do not find cloud “ceilings” at particular values of static stability.

All conclusions here rest upon the behavior of thermal cloud heights, which we are forced to assume are representative of the behavior of visible top heights despite the substantial (and, as yet, unexplained) bias between the two. Future studies may be able to improve on

our results by making use of sufficient quantities of direct information on cloud height from stereoscopic or active sensors.

**Acknowledgments.** We thank Heidi Zeleznik and Jung-Hyo Chae for help with data analysis, and Larry Miloshevich for providing easy access to the raob data from CRYSTAL-FACE. This work was supported by NASA EOS/IDS grant NAG-59632 and NSF grant ATM-0134893.

## References

- Adler, R. F., and R. A. Mack, Thunderstorm cloud top dynamics as inferred from satellite observations and a cloud top parcel model, *J. Atmos. Sci.*, *43*, 1945–1960, 1986.
- Adler, R. F., and A. J. Negri, A satellite infrared technique to estimate tropical convective and stratiform rainfall, *J. Appl. Meteor.*, *27*, 30–51, 1988.
- Alcala, C. M., and A. E. Dessler, Observations of deep convection in the Tropics using the Tropical Rainfall Measuring Mission TRMM precipitation radar, *J. Geophys. Res.*, *107*, art. no.–4792, 2002.
- Burpee, R. W., Peninsula-scale convergence in the south Florida sea breeze, *Mon. Weather Rev.*, *107*, 852–860, 1979.
- Burpee, R. W., and L. N. Lahiff, Area-average rainfall variations on sea-breeze days in south Florida, *Mon. Weather Rev.*, *112*, 520–534, 1984.
- Chen, S. H., and W. Y. Sun, A one-dimensional time dependent cloud model, *J. Meteorol. Soc. Japan*, *80*, 99–118, 2002.
- Ferrier, B. S., and R. A. Houze, One-dimensional time-dependent modeling of GATE cumulonimbus convection, *J. Atmos. Sci.*, *46*, 330–352, 1989.
- Fromm, M. D., and R. Servranckx, Transport of forest fire smoke above the tropopause by supercell convection, *Geophys. Res. Lett.*, *30*, 10.1029/2002GL016,820, 2003.
- Gettelman, A., M. L. Salby, and F. Sassi, Distribution and influence of convection in the tropical tropopause region, *J. Geophys. Res.*, *107*, Art. No. 4080, 2002.
- Grabowski, W. W., MJO-like coherent structures: Sensitivity simulations using the cloud-resolving convection parameterization (CRCP), *J. Atmos. Sci.*, *60*, 847–864, 2003.
- Hartmann, D. L., and K. Larson, An important constraint on tropical cloud–climate feedback, *Geophys. Res. Lett.*, *29*, art. no.–1951, 2002.
- Heysfeld, G. M., R. Fulton, and J. D. Spinhirne, Aircraft overflight measurements of midwest severe storms—implications on geosynchronous satellite interpretations, *Mon. Weather Rev.*, *119*, 436–456, 1991.

- Jensen, E., D. Anderson, H. Selkirk, D. Starr, and O. Toon, Overview of the Cirrus Regional Study of Tropical Anvils and Cirrus Layers - Florida Area Cirrus Experiment (CRYSTAL-FACE), *Bull. Amer. Meteorol. Soc.*, 2003.
- Jensen, M. P., and A. D. Del Genio, Radiative and microphysical characteristics of deep convective systems in the tropical western Pacific, *J. Appl. Meteor.*, 42, 1234–1254, 2003.
- Jorgensen, D. P., and M. A. Lemone, Vertical velocity characteristics of oceanic convection, *J. Atmos. Sci.*, 46, 621–640, 1989.
- Kuang, Z., and C. Bretherton, Convective influence on the heat balance of the tropical tropopause layer: A cloud-resolving model study, *J. Atmos. Sci.*, 2004, submitted manuscript.
- Li, Y., Intensity of convective storms in Florida and their environmental properties, Master's thesis, University of Utah, 2003, 128 pp.
- Lucas, C., E. J. Zipser, and M. A. Lemone, Vertical velocity in oceanic convection off tropical Australia, *J. Atmos. Sci.*, 51, 3183–3193, 1994.
- Miloshevich, L. M., A. Paukkunen, H. Voemel, and S. Oltmans, Development and validation of a time-lag correction for Vaisala radiosonde humidity measurements, *J. Atmos. Oceanic Technol.*, 2004, in Press.
- Minnis, P., L. Nguyen, D. R. Doelling, D. F. Young, W. F. Miller, and D. P. Kratz, Rapid calibration of operational and research meteorological satellite imagers, Part II: Comparison of infrared channels, *J. Atmos. Oceanic Tech.*, 19, 1250–1266, 2002.
- Sherwood, S. C., Convective precursors and predictability in the tropical western Pacific, *Mon. Weather Rev.*, 127, 2977–2991, 1999.
- Sherwood, S. C., and A. E. Dessler, A model for transport across the tropical tropopause, *J. Atmos. Sci.*, 58, 765–779, 2001.
- Sherwood, S. C., T. Horinouchi, and H. A. Zeleznik, Convective impact on temperatures observed near the tropical tropopause, *J. Atmos. Sci.*, 60, 1847–1856, 2003.
- Sherwood, S. C., P. Minnis, M. McGill, and J. Chae, Underestimation of deep convective cloud tops by thermal imagery, *Geophys. Res. Lett.*, 2004, submitted manuscript.

- Souza, E. P., N. O. Renno, and M. A. F. S. Dias, Convective circulations induced by surface heterogeneities, *J. Atmos. Sci.*, 57, 2915–2922, 2000.
- Tompkins, A. M., Organization of tropical convection in low vertical wind shears: The role of water vapor, *J. Atmos. Sci.*, 58, 529–545, 2001.
- Williams, E., et al., Contrasting convective regimes over the Amazon: Implications for cloud electrification, *J. Geophys. Res.*, 107, 10.1029/2001JD000380, 2002.
- Williams, E. R., and N. Renno, An analysis of the conditional instability of the tropical atmosphere, *Mon. Weather Rev.*, 121, 21–36, 1993.
- Yuter, S. E., and R. A. Houze, Three-dimensional kinematic and microphysical evolution of Florida cumulonimbus, Part II: Frequency distributions of vertical velocity, reflectivity, and differential reflectivity, *Mon. Weather Rev.*, 123, 1941–1963, 1995.
- Zipser, E. J., and K. R. Lutz, The vertical profile of radar reflectivity of convective cells—a strong indicator of storm intensity and lightning probability?, *Mon. Weather Rev.*, 122, 1751–1759, 1994.

---

S. Sherwood, Yale University, New Haven, CT 06520 (ssherwood@alum.mit.edu)

Received \_\_\_\_\_

## Figure Captions

**Figure 1.** Mean extinction (in  $\text{m}^{-1}$ ) calculated from the CPL for clouds in three  $T_{11}$  ranges indicated in the legend. Vertical coordinate is height above  $Z_{\text{lid}}(1)$ , the height at which lidar visible optical depth is unity, which is taken to be the visible cloud top. The average position of the GOES  $Z_{11}$  relative to this is also indicated, though this offset is approximate and appears to become greater than indicated as cloud tops approach the tropopause. The vertical dotted line indicates the extinction value corresponding to an ice water concentration equivalent to 5 ppmv, an approximate stratospheric value.

**Figure 2.** PEN region (shaded), KW region (square box), FAGA region (remainder of large box, excluding PEN and KW).

**Figure 3.** Mean temperature sounding from CRYSTAL-FACE.

**Figure 4.** Height distribution of various parameters in the (left to right) PEN, KW, and FAGA regions. Solid lines show  $p_{11}/Z_{11}$  from GOES using three different  $T(Z)$  models: 1) tropopause adiabat (dashes), 2) tropopause + 40hPa adiabat (dot-dash), 3) semiadiabat (dot-dot-dash). Plus/diamond symbols show distribution of pseudo-adiabatic LNB/LMO among parcels below 900 hPa. Mean location of WMO tropopause and cold point are shown by dashed and dotted lines respectively with standard deviations indicated by error bars. Thick dark arrow shows the additional altitude that must be added to  $Z_{11}$  to locate the visible cloud top in most cases; for the tallest clouds the discrepancy appears to increase to that shown by the grey arrow [Sherwood *et al.*, 2004].

**Figure 5.** (Top row) fraction of each region in which GOES  $T_{11} < 235$  K, vs. local time of day. (Second row) the 5th (lower solid) and 0.20th (upper solid) percentile values of  $p_{11}/Z_{11}$  among those points below 235 K. Tropopause and cold point are indicated as in Fig. 4. (Bottom row) variation of CAPE (triangles, left scale) and CIN (squares, left scale divided by ten) with standard errors. CIN values are truncated at 150 J/kg before averaging, to improve the efficiency of the mean statistic (CAPE and CIN diurnal cycle not available for FAGA region). CAPE values are averages over all parcels having values greater than 100 J/kg.

**Figure 6.** As in Fig. 5 except abscissa is day of the month, and moisture variables have been added (scale at right) with \* symbols: upper tropospheric moisture is added to the top row, middle tropospheric to the middle row. FAGA region not included due to lack of sounding information.

**Figure 7.** LNB (top row) and the average of LNB and LMO (bottom row) pressures vs. 0.20th-percentile  $p_{11}$  from GOES, with each day represented by a symbol. Dashed line shows equality, and  $r$  is the correlation coefficient including all points. Though FAGA data are included, LNB and LMO calculations are based on coastal stations and may be inaccurate.

**Figure 8.** GOES  $p_{11}$  minus the mean of LNB and LMO pressures ( $x$ -axis), vs. mean water vapor mixing ratio between 750-500 hPa ( $y$ -axis), for each region. Horizontal bar in left plot shows approximately 1 km of height difference, and the dashed line is drawn through the centroid of the points with a slope of 0.2 times the mean  $y$ -axis value per kilometer. Note that FAGA moisture data are from coastal Florida and will be less representative than those for the other regions.

## Figures

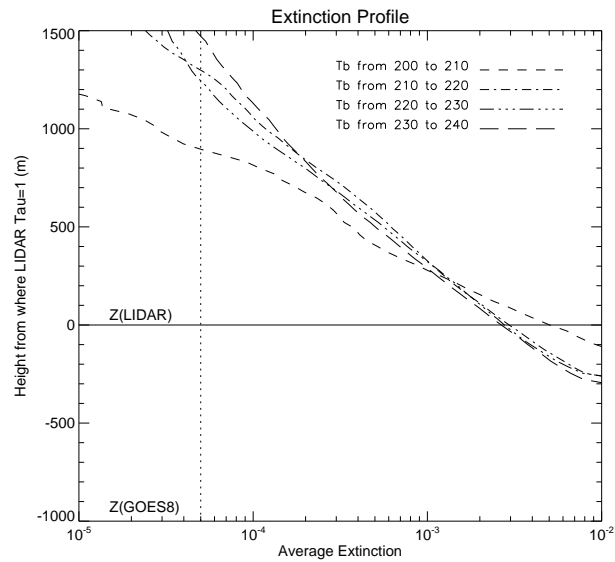


**Figure 1.** Mean extinction (in  $\text{m}^{-1}$ ) calculated from the CPL for clouds in three  $T_{11}$  ranges indicated in the legend. Vertical coordinate is height above  $Z_{\text{lid}}(1)$ , the height at which lidar visible optical depth is unity, which is taken to be the visible cloud top. The average position of the GOES  $Z_{11}$  relative to this is also indicated, though this offset is approximate and appears to become greater than indicated as cloud tops approach the tropopause. The vertical dotted line indicates the extinction value corresponding to an ice water concentration equivalent to 5 ppmv, an approximate stratospheric value.

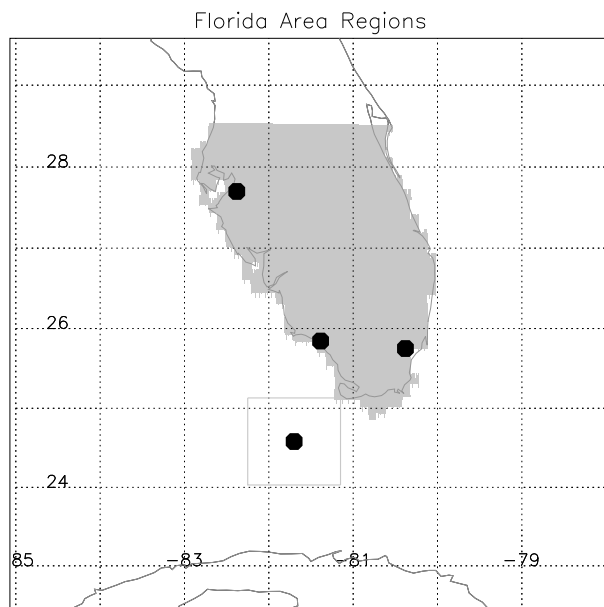


**Figure 2.** PEN region (shaded), KW region (square box), FAGA region (remainder of large box, excluding PEN and KW).

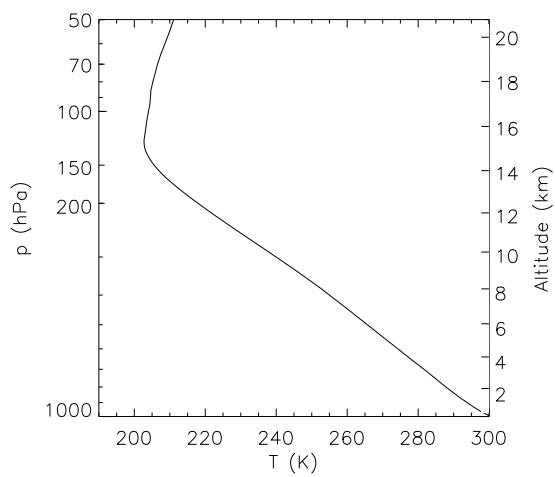


**Figure 3.** Mean temperature sounding from CRYSTAL-FACE.

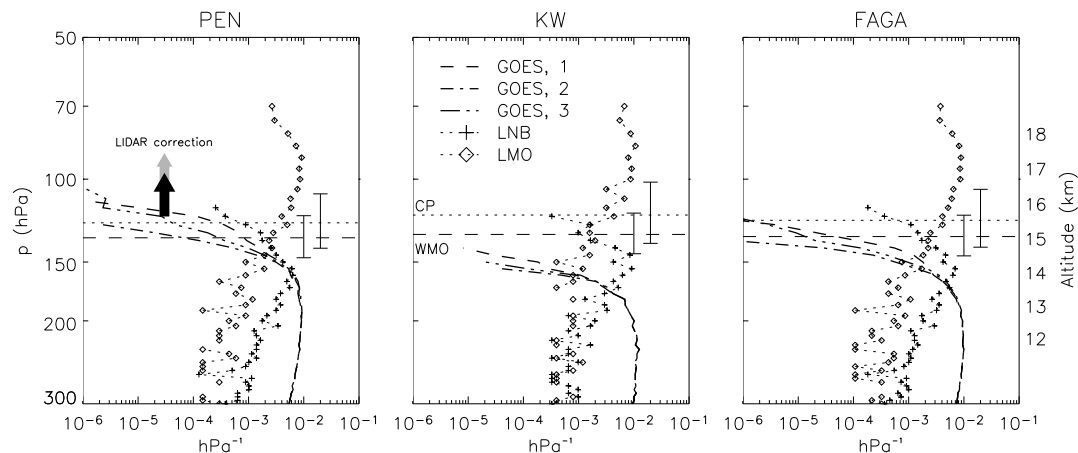


**Figure 4.** Height distribution of various parameters in the (left to right) PEN, KW, and FAGA regions. Solid lines show  $p_{11}/Z_{11}$  from GOES using three different  $T(Z)$  models: 1) tropopause adiabat (dashes), 2) tropopause + 40hPa adiabat (dot-dash), 3) semiadiabat (dot-dot-dash). Plus/diamond symbols show distribution of pseudo-adiabatic LNB/LMO among parcels below 900 hPa. Mean location of WMO tropopause and cold point are shown by dashed and dotted lines respectively with standard deviations indicated by error bars. Thick dark arrow shows the additional altitude that must be added to  $Z_{11}$  to locate the visible cloud top in most cases; for the tallest clouds the discrepancy appears to increase to that shown by the grey arrow [Sherwood *et al.*, 2004].

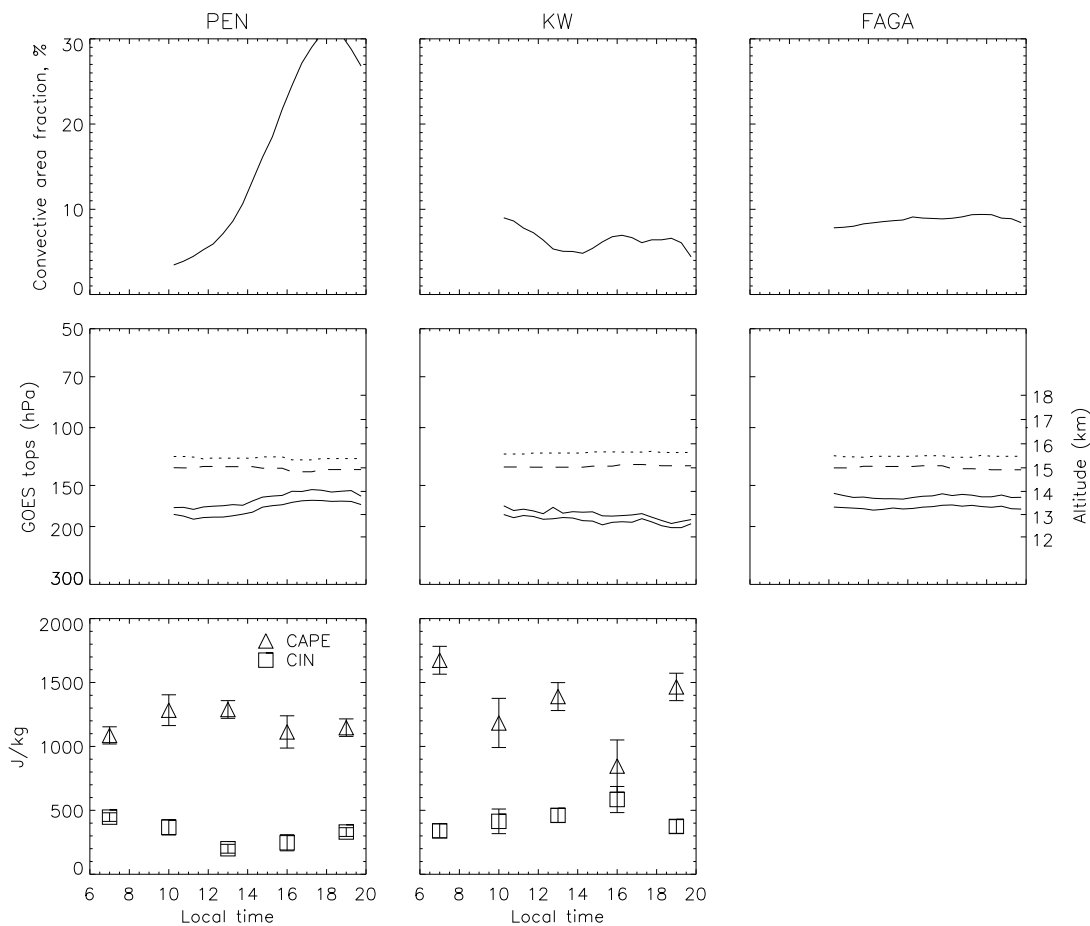


**Figure 5.** (Top row) fraction of each region in which GOES  $T_{11} < 235$  K, vs. local time of day. (Second row) the 5th (lower solid) and 0.20th (upper solid) percentile values of  $p_{11}/Z_{11}$  among those points below 235 K. Tropopause and cold point are indicated as in Fig. 4. (Bottom row) variation of CAPE (triangles, left scale) and CIN (squares, left scale divided by ten) with standard errors. CIN values are truncated at 150 J/kg before averaging, to improve the efficiency of the mean statistic (CAPE and CIN diurnal cycle not available for FAGA region). CAPE values are averages over all parcels having values greater than 100 J/kg.

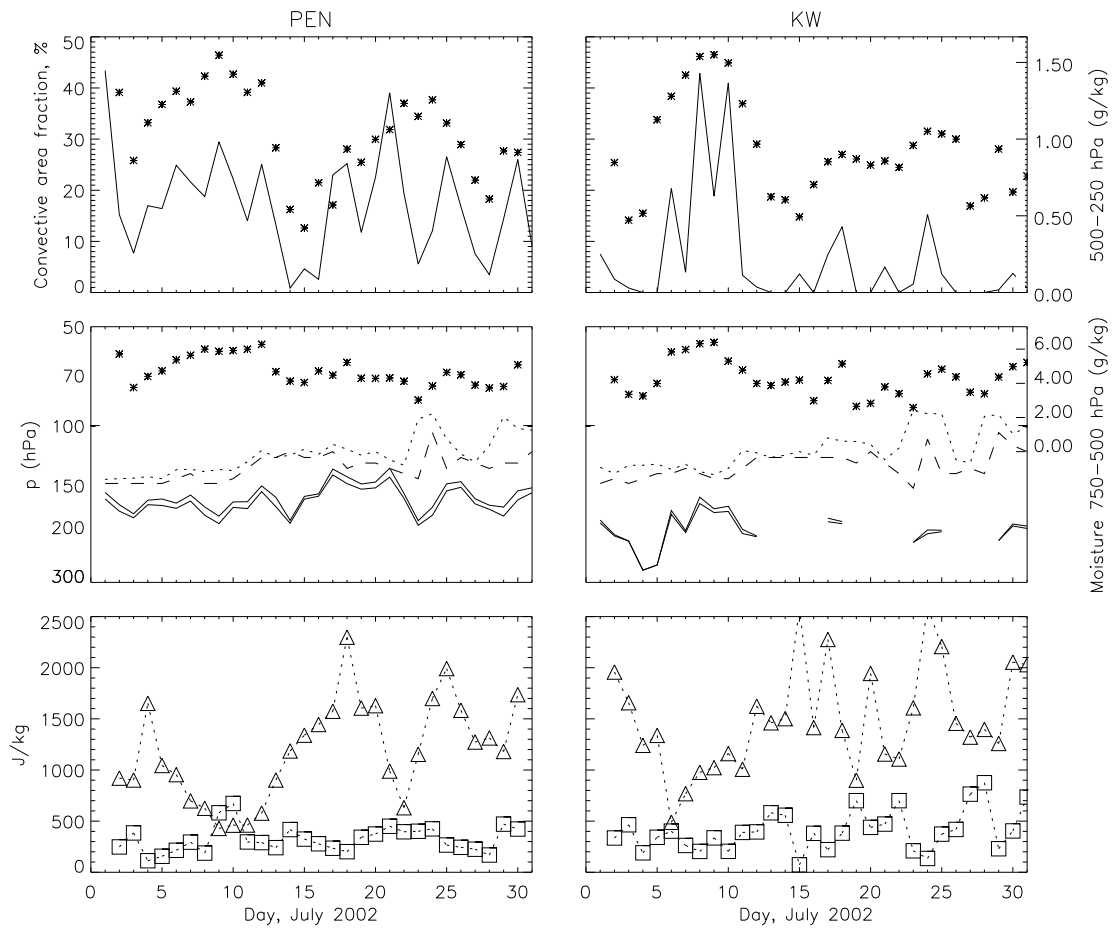


**Figure 6.** As in Fig. 5 except abscissa is day of the month, and moisture variables have been added (scale at right) with \* symbols: upper tropospheric moisture is added to the top row, middle tropospheric to the middle row. FAGA region not included due to lack of sounding information.

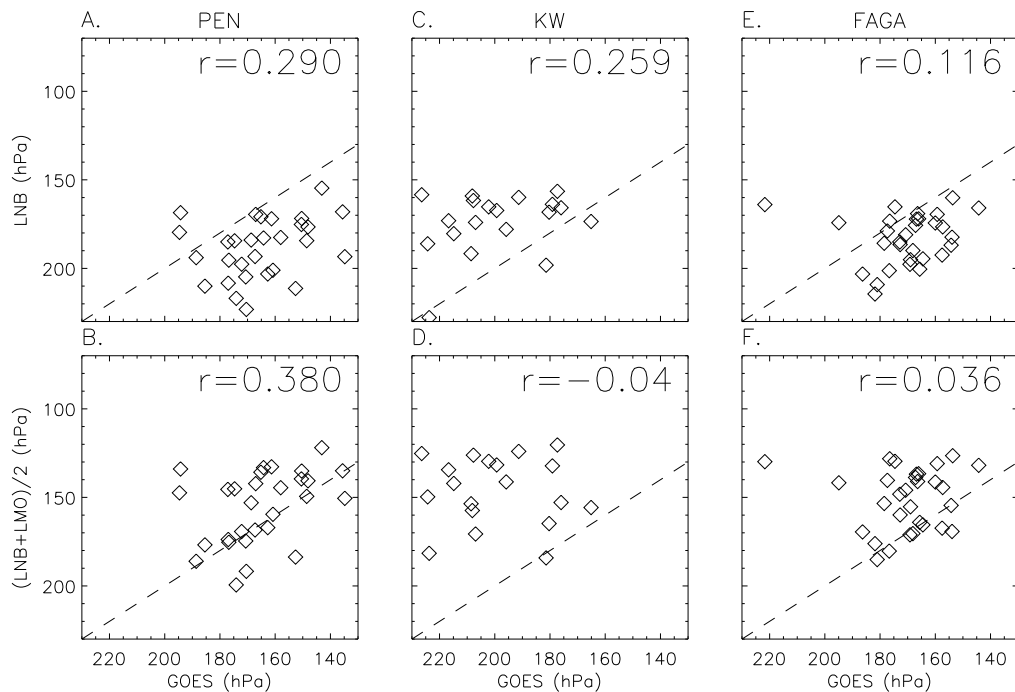


**Figure 7.** LNB (top row) and the average of LNB and LMO (bottom row) pressures vs. 0.20th-percentile  $p_{11}$  from GOES, with each day represented by a symbol. Dashed line shows equality, and  $r$  is the correlation coefficient including all points. Though FAGA data are included, LNB and LMO calculations are based on coastal stations and may be inaccurate.

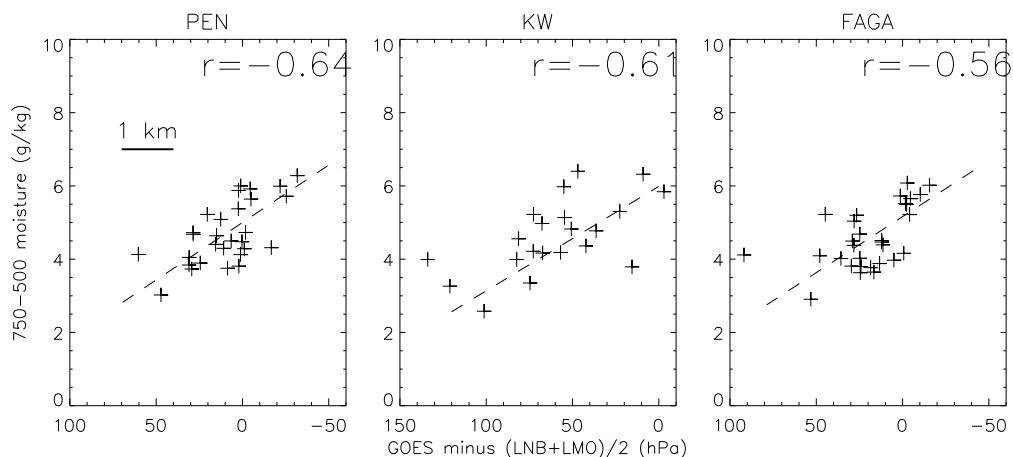


**Figure 8.** GOES  $p_{11}$  minus the mean of LNB and LMO pressures ( $x$ -axis), vs. mean water vapor mixing ratio between 750–500 hPa ( $y$ -axis), for each region. Horizontal bar in left plot shows approximately 1 km of height difference, and the dashed line is drawn through the centroid of the points with a slope of 0.2 times the mean  $y$ -axis value per kilometer. Note that FAGA moisture data are from coastal Florida and will be less representative than those for the other regions.